WILEY-VCH

Instability of gas-phase-assembled Pd-Fe alloy nanoparticles under ambient conditions: Pd/FeOx core–shell formation and magnetic and hydrogen-sensing consequences

Moisés G. Zarzoza Medina, Raúl López-Martín, Benito Santos Burgos, Santiago Ceballos, Óscar J. Durá 1, Irene Morales, Beatrice Muzzi, José F. Marco, Miguel A. Arranz, Panagiotis Grammatikopoulos, Daniel Salazar, Peter S. Normile, José A. De Toro**

E-mail: moisesg.zarzoza@uclm.es

joseangel.toro@uclm.es

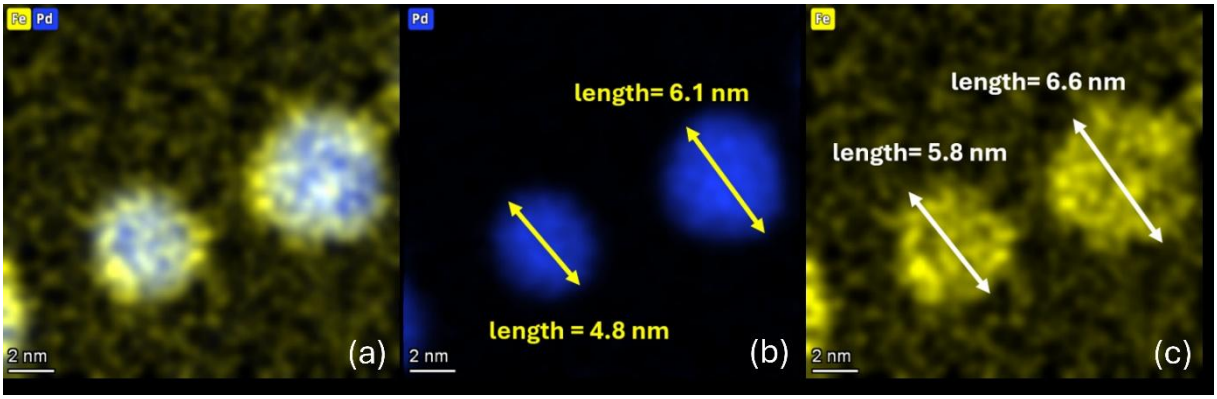

Figure S1. Additional STEM-EDX elemental maps of representative FePd nanoparticles showing the spatial distribution of Fe and Pd. In all cases, the Fe signal extends to the particle edges while the Pd signal remains confined to the inner region, consistently supporting the core–shell architecture with a Pd-rich core and an Fe-rich shell. The scale bar is 2 nm.

Table S1. Peak positions of the fitted components of the XPS spectra at different edges for the pure Pd target, Pd NPs and the NP films of different Fe contents prepared with and without a Nb matrix.

Sample	Pd $3d_{5/2}$	Pd $3d_{3/2}$	Fe $2p_{3/2}$	Fe $2p_{1/2}$
Target-Pd	335.26 Pd	340.55 Pd		
	336.07 PdO	341.45 PdO		
Pd NPs	335.67 Pd	340.92 Pd		
	336.57 PdO	341.93 PdO		
	338.38 PdO_2	343.23 PdO_2		
Pd-Fe NPs	335.87 Pd	341.16 Pd	707.80 Fe	720.90 Fe
	336.88 PdO	342.34 PdO	709.02 Fe^{2+}	722.12 Fe^{2+}
			710.93 Fe^{3+}	723.97 Fe^{3+}
			714.66 Fe^{2+} Sat	727.69 Fe^{2+} Sat
			719.41Fe^{3+} Sat	732.61 Fe^{3+} Sat
PdFe@Nb	336.09 Pd	341.42 Pd	706.74 Fe	719.47 Fe
			710.13 FeO_x	722.17 FeO_x

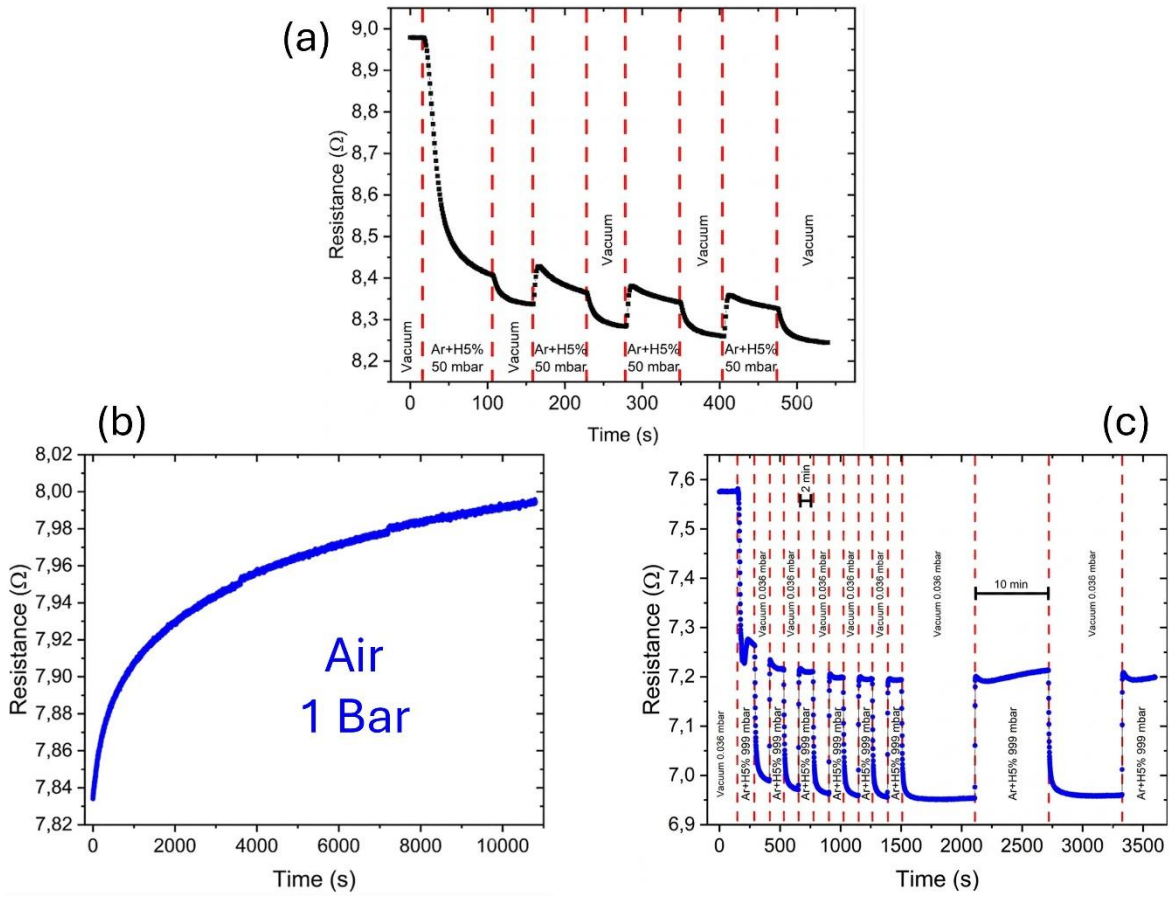

Figure S2. (a) Dynamic resistance response of the porous NP film during multiple cycles of exposure to 5% H_2/Ar (room temperature). (b) Resistance increase upon exposure to ambient air, indicating reoxidation of the FeO_x shell. (c) Subsequent H_2/Ar cycles after air exposure, showing the reappearance of the decaying background behavior attributed to progressive reduction of the FeO_x shell.